Science Advances
AAAS

advances.sciencemag.org/cgi/content/full/6/22/eaaz6433/DC1

Supplementary Materials for

Reducing the aerosol forcing uncertainty using observational constraints on warm rain processes

Johannes Mülmenstädt*, Christine Nam, Marc Salzmann, Jan Kretzschmar, Tristan S. L'Ecuyer, Ulrike Lohmann, Po-Lun Ma, Gunnar Myhre, David Neubauer, Philip Stier, Kentaroh Suzuki, Minghuai Wang, Johannes Quaas

*Corresponding author. Email: johannes.muelmenstaedt@pnnl.gov

Published 29 May 2020, *Sci. Adv.* **6**, eaaz6433 (2020)
DOI: 10.1126/sciadv.aaz6433

This PDF file includes:

Texts S1 to S5
Figs. S1 to S9
Tables S1 to S3
References

Text S1: Positive and negative adjustments

Processes that lead to enhanced evaporation of smaller droplets in polluted conditions involve mixing of drier ambient air into clouds at cloud top (*8*, *9*, *75*, *76*) and cloud sides (*10*, *77*), as well as responses in cloud-scale and cloud-field-scale dynamics (*27*, *78*, *79*). These cloud responses are difficult to parameterize in GCMs because they occur at length scales typical of turbulent processes (centimeters through kilometers) through mesocale processes (kilometers to tens of kilometers), with abundant feedbacks across scales that are implicitly represented, at best, by GCM parameterizations. Processes that lead to precipitation suppression by increased droplet number concentration in polluted clouds, on the other hand, can be parameterized entirely at the cloud droplet scale within the microphysical warm-phase precipitation processes (see Methods). These cloud responses are explicitly, albeit crudely, represented in many GCMs (*80*–*83*).

Text S2: Caveats

We are not suggesting that the tuning strategies explored here are optimal; they are not able to reduce the warm-rain bias to zero, nor are they free from compensating biases elsewhere in the model – as shown by the need for scale factors smaller than unity, opposite to the enhancement factors needed to correct for subgrid variability in liquid water content (*61*, *84*). Rather, we have chosen these strategies to explore the parameter space of possible model behavior if the far more involved task of addressing base precipitation process behavior biases were undertaken. These simple experiments suffice to document the likely rewards in reduced base-process-induced $\mathrm{ERF_{aci}}$ uncertainty and reduced equifinality-induced parameter degeneracy and to elicit the improvements in modeling, observations, and model–observation intercomparison techniques required to realize said rewards.

We also acknowledge that f_{warm} would ideally be superseded by a diagnostic that does not mix warm and cold rain processes, such as the warm-rain probability conditioned on the presence of cloud p_{warm}. We have chosen f_{warm} to simplify future comparison of ECHAM–HAMMOZ with other models that do not implement radar simulators. In these models, a threshold surface rain rate must be chosen below which the grid box is considered nonprecipitating. The uncertainty associated with the choice of threshold largely cancels in the ratio $p_{\mathrm{warm}}/(p_{\mathrm{warm}} + p_{\mathrm{cold}}) = f_{\mathrm{warm}}$; if the intensity spectra of warm and cold rain matched, the cancellation would be exact. However, observations indicate so little warm rain in the extratropics compared to the model that the magnitude of the denominator in f_{warm} is relatively unimportant to the constraint mechanism there; the constraint is simply that warm rain should not occur in those regions. Fortuitously, the adjustments in the model also predominantly occur in the polluted northern-hemisphere extratropics (*41*). Nonetheless, we advocate rapid adoption of satellite simulators by all models, a cobenefit of which is that this analysis can be refined using p_{warm}.

Finally, we acknowledge that large TOA imbalances, while a necessary evil in these sensitivity studies (see Text S3), are unacceptable in a production model. Thus, reducing the large model bias in autoconversion will require a similarly large retuning elsewhere, which will have to be accomplished without introducing or worsening biases in other state variables. We surmise that revisions that enhance the accretion of cloud water to rain droplets may be a promising avenue, simultaneously acting as a sink for the excess $\mathcal{L}$ resulting from reduced autoconversion, strengthening the intensity and reducing the frequency of precipitation, and bringing the autoconversion–accretion partitioning into better agreement with observations (*14*, *85*, *86*).

Text S3: Rapid-adjustment metrics

It is inherently difficult to quantify the change in $\mathrm{ERF_{aci}}$ components in a GCM when parameterized processes are changed. There are two reasons for this. The first reason is that, for many applications, it is desirable for the model to reproduce the PD state of the atmosphere as closely as possible; this is especially true in coupled atmosphere–ocean climate runs, where an energy imbalance in the model will result in a drift of heat content of the climate system over time. Changing one process in isolation, even if it happens to make that process more realistic, is likely to bring the atmospheric state, including the energy balance, into worse overall agreement than what had been achieved previously by careful tuning. Thus, the model is often retuned after implementing the process change, so that the overall quality of the model is not degraded. However, even apparently unrelated parameter changes used for retuning can impact the $\mathrm{ERF_{aci}}$ and its components, masking the effect of the intentional process change (*19*). To avoid this problem, we choose not to retune the model for these experiments. In fixed-SST, nudged simulations, the model climate cannot diverge far from its control climate.

However, we still run into a second reason why quantifying $\mathrm{ERF_{aci}}$ components is difficult; namely, that the $\mathrm{ERF_{aci}}$ components depend on the model base state, and changing the process formulations changes the base state. Assume that the model can be described by a vector of processes $\boldsymbol{p}$ and a vector of state variables $\boldsymbol{x}$. The processes map the state variables onto rates of change of the state variables. In general, the state variables will depend on the processes through an unknown functional ξ:

$$\boldsymbol{x} = \xi(\boldsymbol{p}); \tag{S3.1}$$

reformulating the processes so that $\boldsymbol{p} \to \boldsymbol{p}'$ will therefore change the state vector as well.

Further assume that $F_{\mathcal{L}}$ can be decomposed into a factor $\mathcal{S}$ that explicitly depends only on the state variables and a factor $\mathcal{F}_{\mathcal{L}}$ that depends only on processes:

$$F_{\mathcal{L}}(\boldsymbol{p},\boldsymbol{x}) = \mathcal{F}_{\mathcal{L}}(\boldsymbol{p}) \times \mathcal{S}(\boldsymbol{x}). \tag{S3.2}$$

Our aim is to find another variable Φ that does not depend explicitly on p and depends on x in the same way as $F_{\mathcal{L}}$, i.e., $\Phi(\boldsymbol{x}) \propto \mathcal{S}(\boldsymbol{x})$. If we can identify such a variable, the ratio $F_{\mathcal{L}}/\Phi \propto \mathcal{F}_{\mathcal{L}}(\boldsymbol{p})$ can be used to diagnose the response of the adjustments to the change in process formulation, free from the confounding effect of unrelated state variable changes $\boldsymbol{x} \to \boldsymbol{x}'$.

The assumption that a factorization of the form (S3.2) is possible can be rationalized for changes in model formulation that result in small changes in $\boldsymbol{x}$ by the following argument. Suppose we artificially made clouds more reflective while keeping the processes affecting $\mathcal{F}_{\mathcal{L}}$ the same, e.g., by introducing a perturbation in N_d that is visible only to the radiation scheme; this would leave $\mathcal{F}_{\mathcal{L}}$ unchanged by construction but still change $F_{\mathcal{L}}$ due to the increased cloud albedo encapsulated in a change in $\mathcal{S}$.

A more difficult step is identifying candidates for Φ. The preceding proportionality argument suggests that a desirable property of Φ is covariability with cloud albedo change. An initial set of candidates might therefore include $\mathcal{L}$, which strongly controls cloud albedo; and the shortwave cloud radiative effect $\mathcal{S}_c = S^{\mathrm{all}} - S^{\mathrm{clr}}$, i.e., the difference in solar-spectrum radiative flux at the model top of atmosphere between all-sky and clear-sky conditions, which converts the change in cloud albedo into a radiative flux perturbation. While there is indeed a very tight relationship between $\mathcal{L}$ and albedo across all our model configurations, the albedo saturates at high $\mathcal{L}$, which reduces its utility as a normalization for radiative quantities.

We consider a further candidate for Φ: the radiative forcing F_{N_d}. The process changes we have made do not affect F_{N_d} explicitly, satisfying one of our above criteria for Φ. The state variable changes induced by the process changes do affect F_{N_d}, however, in that the cloud albedo response to a given N_d perturbation is a nonlinear function of $\mathcal{L}$ and N_d. We surmise that the dependence of F_{N_d} and $F_{\mathcal{L}}$ on $\boldsymbol{x}$ are better analogs than the dependence of $\mathcal{S}_c$. The reason is that both components of $\mathrm{ERF_{aci}}$ are sensitive to the spatial covariability of cloud changes and anthropogenic aerosol perturbations (*41*), whereas $\mathcal{S}_c$ is not; both components are affected by the greater anthropogenic N_d perturbation per unit emissions that results from reduced wet scavenging when precipitation probability is reduced; and the sensitivity of both components to changes in $\mathcal{L}$ and N_d saturates in a higher-$\mathcal{L}$, higher-N_d state. Evidence for proportionality between F_{N_d} and $F_{\mathcal{L}}$ in GCMs is presented based on spatial correlations in Mülmenstädt *et al.* (*41*) and on intermodel correlation in Gryspeerdt *et al.* (*42*).

Based on these arguments, we use the normalized adjustment $F_{\mathcal{L}}/F_{N_d}$ in this paper. To test the robustness of our conclusions to this choice, Fig. S8 reproduces Fig. 3 for the other normalization choices we have considered, $\Phi \in \{\mathcal{L}, \mathcal{S}_c\}$; Tables S1–S3 list the global-mean $\mathrm{ERF_{aci}}$ components and state variables. For all three metrics, there is a bifurcation in the adjustment response to reduced f_{warm} bias; the Q_{aut} scaling reduces the adjustment strength according to all three metrics, while the r_e threshold tuning increases the adjustment strength according to the $F_{\mathcal{L}}/F_{N_d}$ and $F_{\mathcal{L}}/\mathcal{S}_c$ metrics and causes little change according to the $F_{\mathcal{L}}/\mathcal{L}$ metric. Thus, the conclusion that an observational constraint on the rapid adjustment depends on knowing whether to address the drizzle bias or the rain bias appears robust to the choice of Φ. For all three metrics, increasing β (i.e., tuning in the direction of stronger susceptibility) results in adjustment changes that are comparable to the experiments modifying parameters that control base process behavior (α, γ, r_c); for all three metrics, large increases in β, which should correspond to greater process susceptibility, results in weaker adjustment (see also Text S5). Thus, the conclusion that the base precipitation process behavior and the process susceptibility are both important contributors to the projected adjustment also appears robust to the choice of Φ.

Text S4: Geographic patterns of adjustment changes

Figure S4 shows the geographic distribution of the changes in normalized adjustment when the scale factor is reduced and when the r_e threshold is increased; the most drastic retuning is chosen in each case to produce clear patterns in the presence of statistical noise.

In the scale factor experiment, the change in normalized adjustment is robustly negative in the northern-hemisphere extratropics. Given the decrease in warm rain in these regions, this change is consistent with our hypothesis that base process behavior leading to reduced warm rain reduces $F_{\mathcal{L}}$. In the Sc regions, where cold rain is exceedingly rare, warm rain is still the dominant form of precipitation even with a reduced scale factor; here, the sign is reversed, presumably because the Golaz *et al.* (*19*) applies; see below.

In the r_e threshold experiment, there is a robust increase in $F_{\mathcal{L}}/F_{N_d}$ over oceans. This is in accordance with the Golaz *et al.* (*19*) argument. To summarize the argument, we first note that effective radius and liquid-water mixing ratio are related:

$$q_l = \frac{4}{3}\pi\frac{\rho_l}{\rho}r_e^3 N_d, \tag{S4.1}$$

where ρ_l is the density of water and ρ is the density of air; strictly, the relationship holds for the volumetric-mean radius (by definition), but the ratio between r_e and volumetric radius is close to unity. Next, we note that precipitation is a sufficiently important sink of q_l in the model that reducing the ability of clouds to precipitate below a threshold r_e (or equivalently q_l) causes cloud water to build up until the new, higher threshold is reached. The mean q_l is thus strongly controlled by the threshold r_e:

$$q_l \sim \frac{4}{3}\pi\frac{\rho_l}{\rho}r_c^3 N_d. \tag{S4.2}$$

An anthropogenic N_d perturbation ΔN_d thus leads to a q_l response that is proportional to r_c^3:

$$\Delta q_l \sim \frac{4}{3}\pi\frac{\rho_l}{\rho}r_c^3 \Delta N_d, \tag{S4.3}$$

so that models with higher r_c will have a stronger q_l response to a give anthropogenic aerosol perturbation than models with lower r_c.

For this argument to work, the moisture must not be limited by source processes, such as limits on surface evaporation, or other sink processes, such as consumption by parameterized convection. Over oceans, where Fig. S4 shows an increase in $F_{\mathcal{L}}/F_{N_d}$, we expect the moisture supply to be unrestricted. Figure S4 also shows a reduction in $F_{\mathcal{L}}/F_{N_d}$ over parts of the continents, which may be explained by a lower evaporative flux or a more convective atmosphere that limits the applicability of the Golaz *et al.* (*19*) argument.

Text S5: Susceptibility versus base process behavior

The thinking underlying Wang *et al.* (*27*) is that the susceptibility of precipitation to aerosol (*87*) controls the model estimate of $F_{\mathcal{L}}$. Accordingly, some modeling studies find that varying β, which changes the susceptibility of precipitation to aerosol, is the main control on $\mathrm{ERF_{aci}}$ (*88*, *89*). The difficulty of diagnosing $F_{\mathcal{L}}$ separately from other components of $\mathrm{ERF_{aci}}$, as well as the retuning process after perturbing a parameter of the model (*90*), complicates the assessment to what extent $F_{\mathcal{L}}$ responds to changes in β in such studies (see also Text S3).

A more detailed calculation of the process susceptibility (*91*, *92*) shows that β is not the only contribution to the autoconversion rate susceptibility to N_d; rather, the susceptibility receives contributions both from exponents in (2):

$$\frac{d\ln Q_{\mathrm{aut}}}{d\ln N_d} = -\beta + \alpha\frac{d\ln q_l}{d\ln N_d}, \tag{S5.1}$$

i.e., the susceptibility both influences and depends on rapid adjustments ($d \ln q_l / d \ln N_d$, in a global-mean sense, controlling $F_{\mathcal{L}}$). In light of the model diversity in $F_{\mathcal{L}}$ estimates (*42*), we can assume that the relative contribution of β to the process susceptibility will also be diverse. These considerations notwithstanding, $F_{\mathcal{L}}/F_{N_d}$ *decreases* at large β, when the process susceptibility should be maximal, indicating that the presence of multiple terms in (S5.1) is not the dominant source of the insensitivity of the rapid adjustments to β in this model. A more likely explanation is that the components of $\mathrm{ERF_{aci}}$ are emergent properties of a complex system (*83*), so we should not expect a straightforward correspondence between $F_{\mathcal{L}}$ and process rates or susceptibility (*93*).

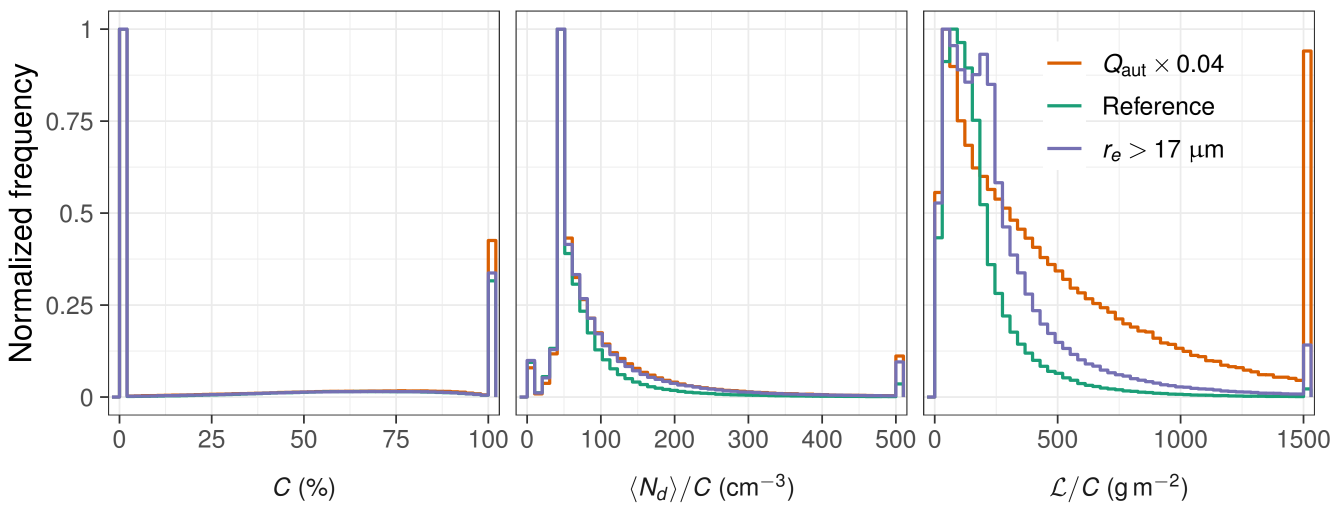

Figure S1. Distributions of cloud properties in different experiments.
Distributions of C, $\langle N_d \rangle / C$, and $\mathcal{L}/C\}$ are shown, where C is the two-dimensional projected liquid-cloud fraction, and $\langle N_d \rangle$ is the vertical average of N_d over the liquid cloud column; the normalization by C is chosen to approximate an "in-cloud" liquid water path and "in-cloud" droplet number concentration, although the concept is not well defined in clouds spanning multiple model levels. Frequencies are normalized to the mode of the frequency distribution.

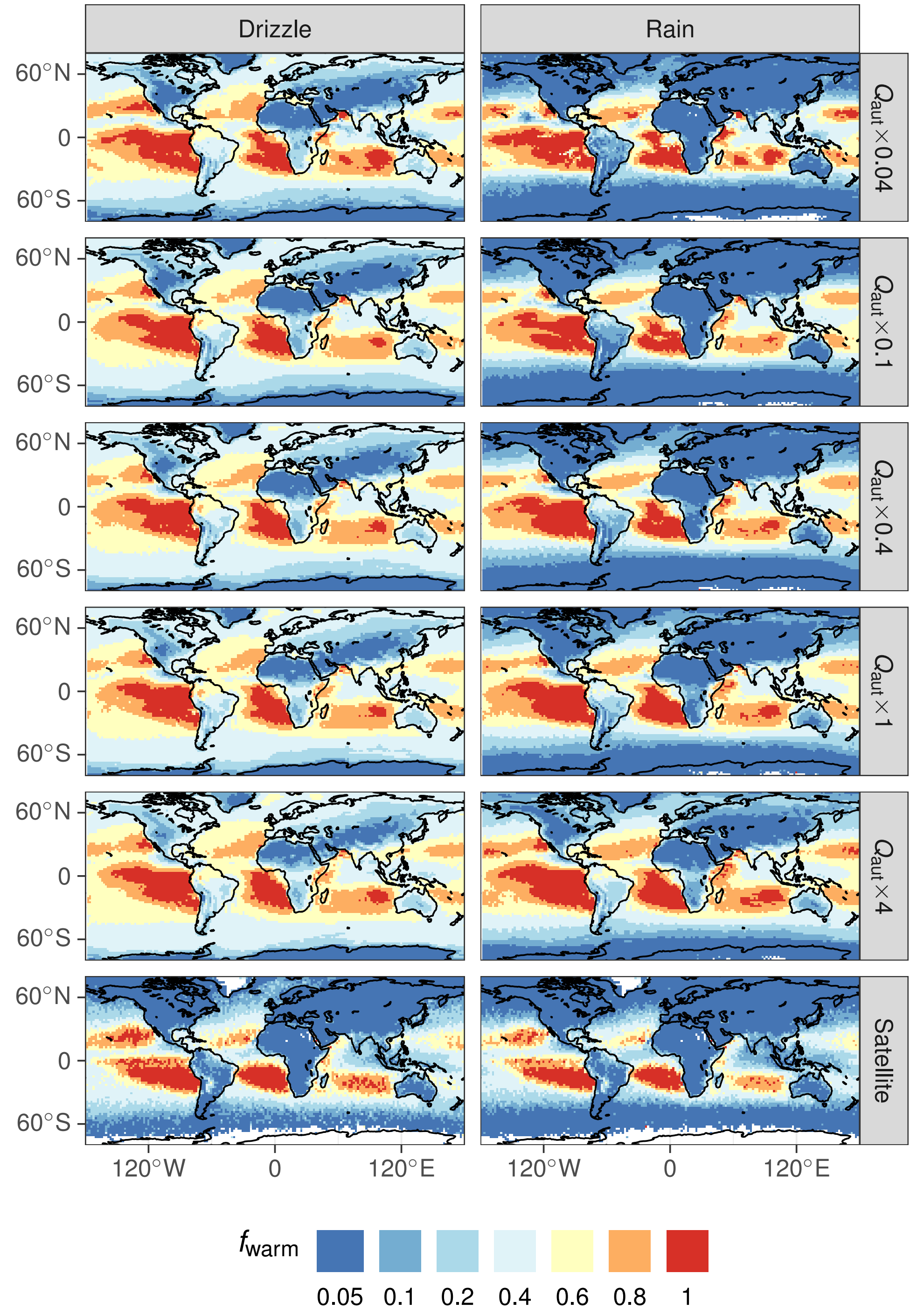

Figure S2. Warm-rain fraction from satellite and model in various scaling configurations.
The reference configuration is $Q_{aut} \times 4$. As the scale factor is reduced, warm rain decreases rapidly, but warm drizzle is relatively unaffected.

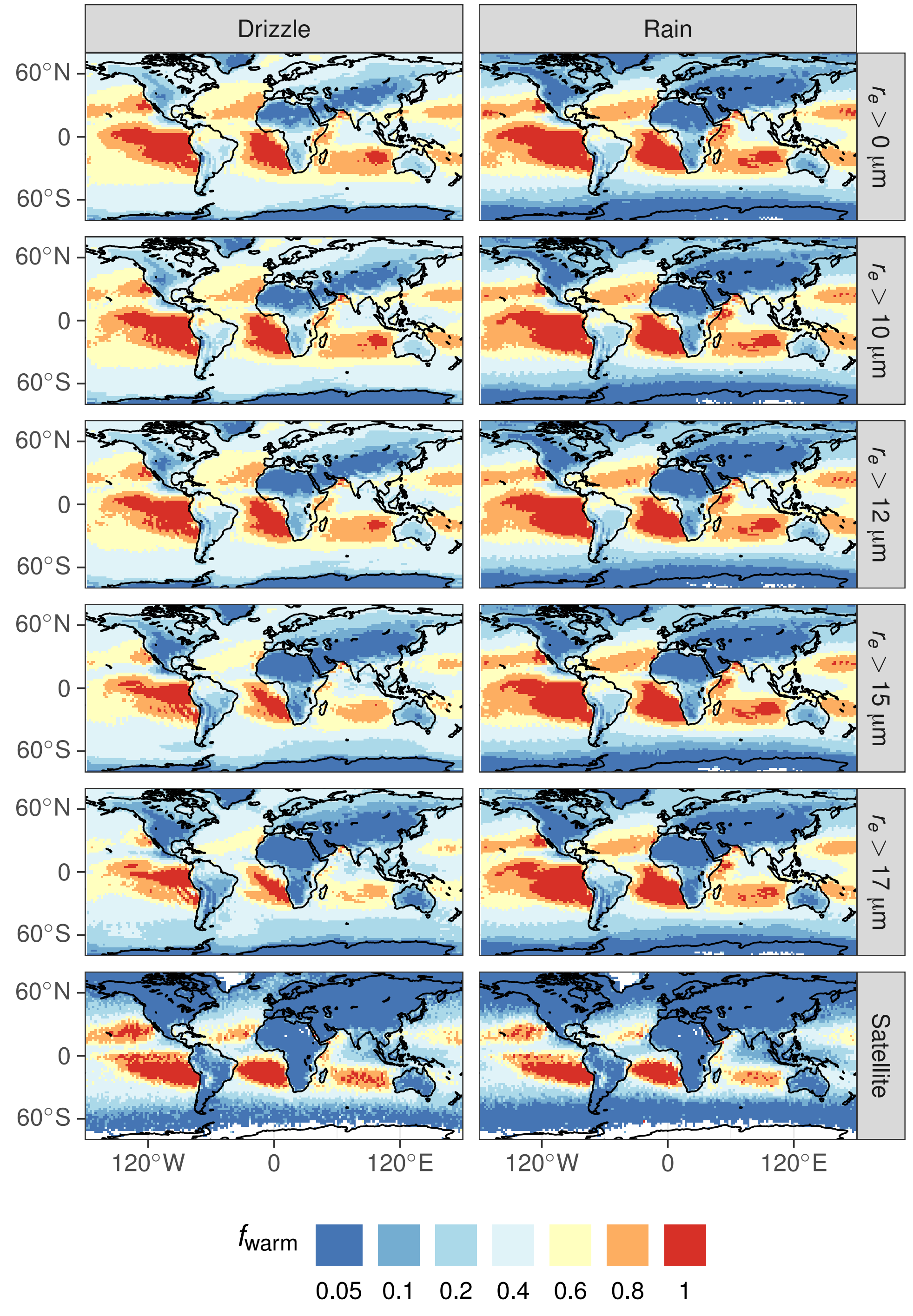

Figure S3. Warm-rain fraction from satellite and model in various r_e threshold configurations.
The reference configuration is $r_e > 0$. As the threshold is increased, warm drizzle decreases rapidly, but warm rain is relatively unaffected.

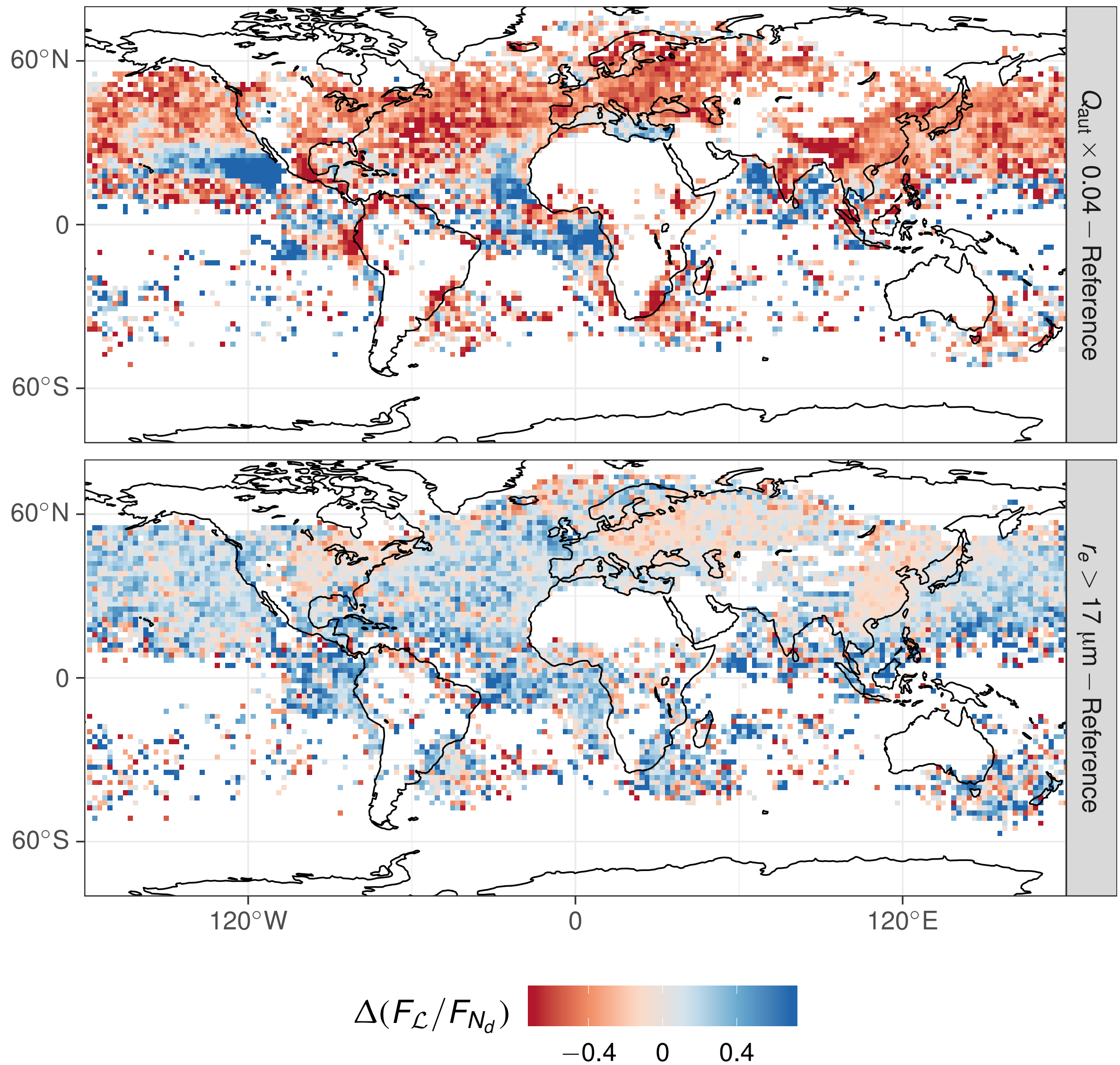

Figure S4. Geographic distribution of the change in normalized adjustment.
$F_{\mathcal{L}}/F_{N_d}$ in the $Q_{\mathrm{aut}} \times 0.04$ and $r_e > 17$ μm experiments is shown relative to the reference configuration.

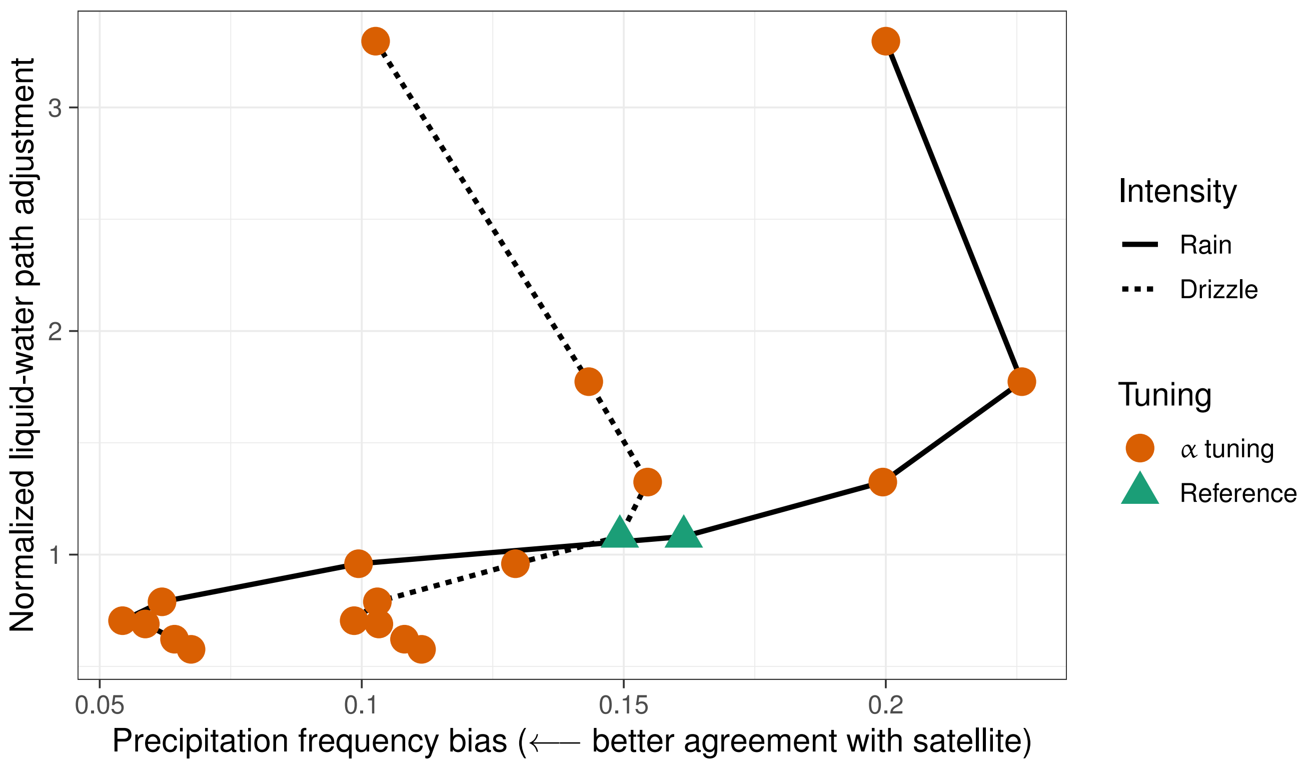

Figure S5. The relationship between $f_{\mathbf{warm}}$ bias and $F_{\mathcal{L}}/F_{N_d}$ when varying α.
This figure reprises Fig. 3 but varies α instead of r_c and γ.

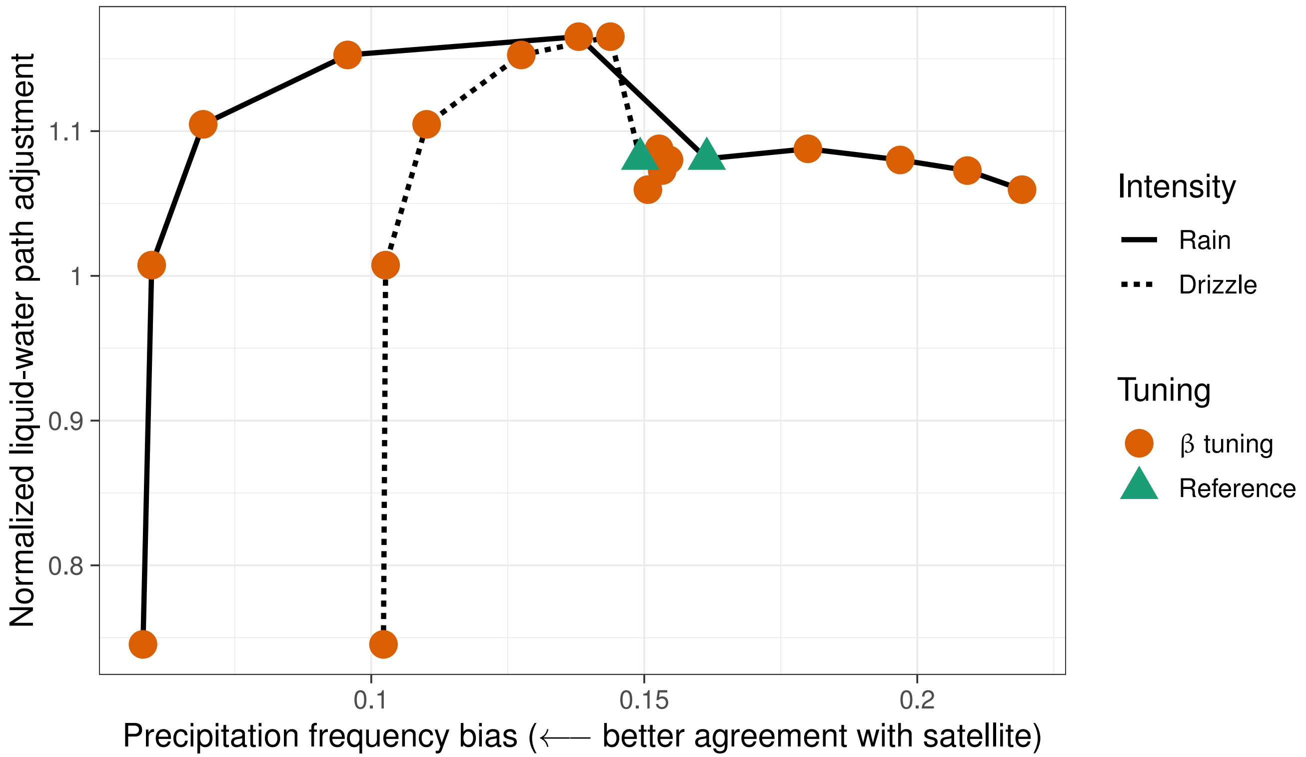

Figure S6. The relationship between f_{warm} bias and $F_{\mathcal{L}}/F_{N_d}$ when varying β.
This figure reprises Fig. 3 but varies β instead of r_c and γ.

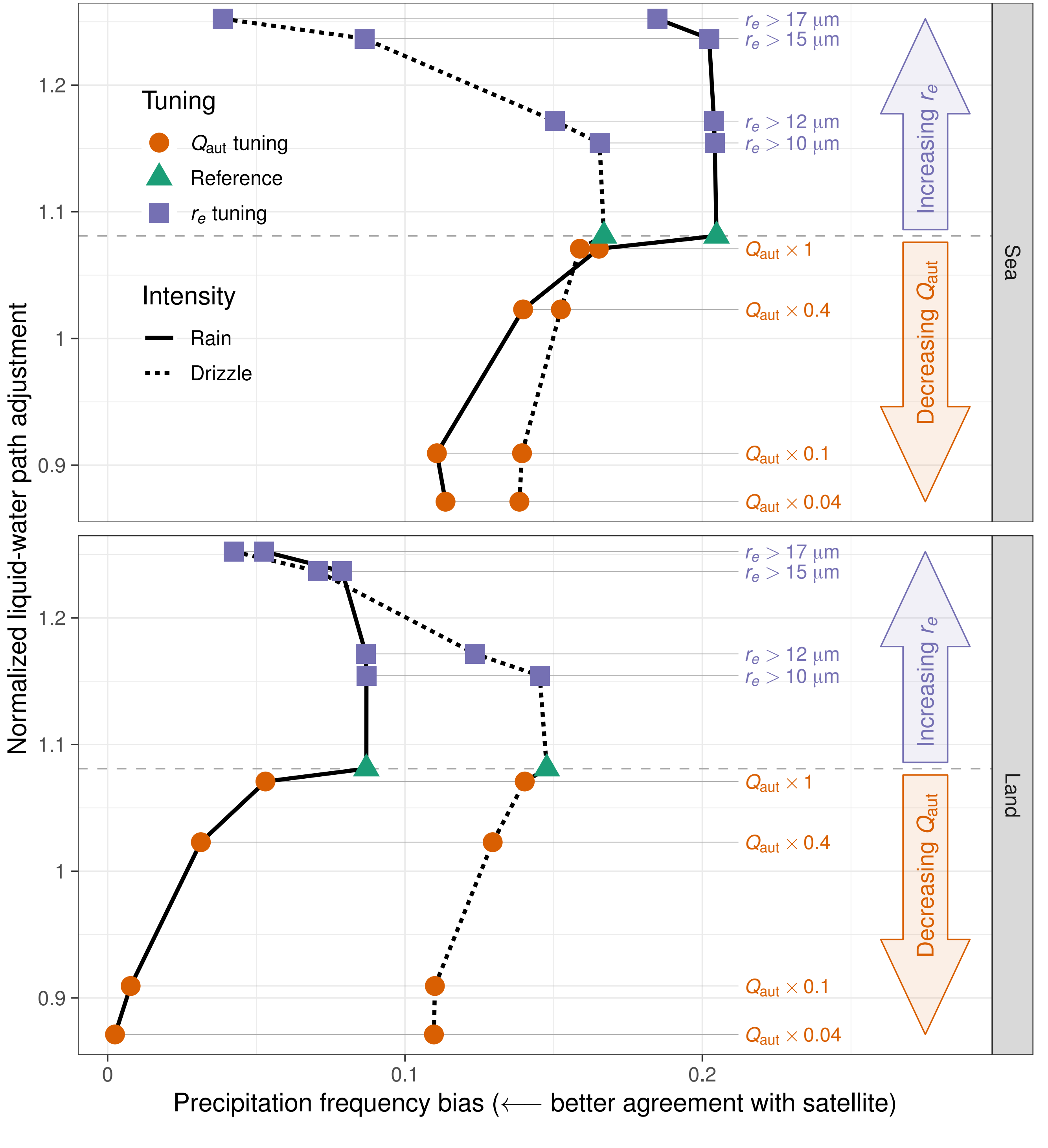

Figure S7. The relationship between f_{warm} bias and $F_{\mathcal{L}}/F_{N_d}$ over land and ocean.
This figure reprises Fig. 3 but separates the $F_{\mathcal{L}}/F_{N_d}$ responses over land and ocean.

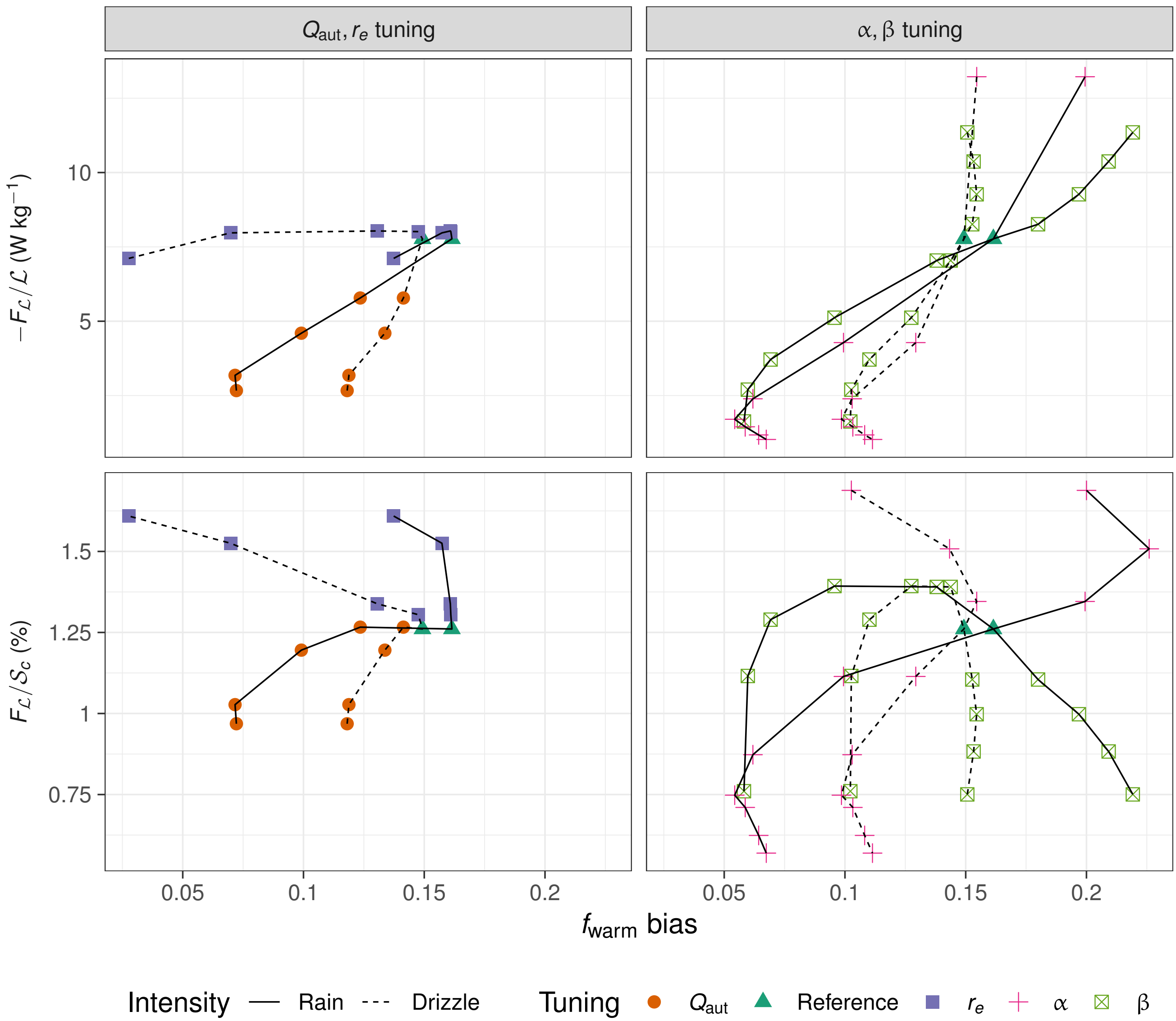

Figure S8. The relationship between f_{warm} bias and multiple adjustment metrics.
This figure reprises Figs. 3, S5, and S6, but for alternate adjustment metrics $-F_{\mathcal{L}}/\mathcal{L}$ (the negative prefactor is chosen so that a larger value of the metric indicates a stronger adjustment, in common with the other metrics) and $F_{\mathcal{L}}/\mathcal{S}_c$. (Note that the $\alpha \in \{1.75, 2\}$ data points are off scale in the $-F_{\mathcal{L}}/\mathcal{L}$ panel.)

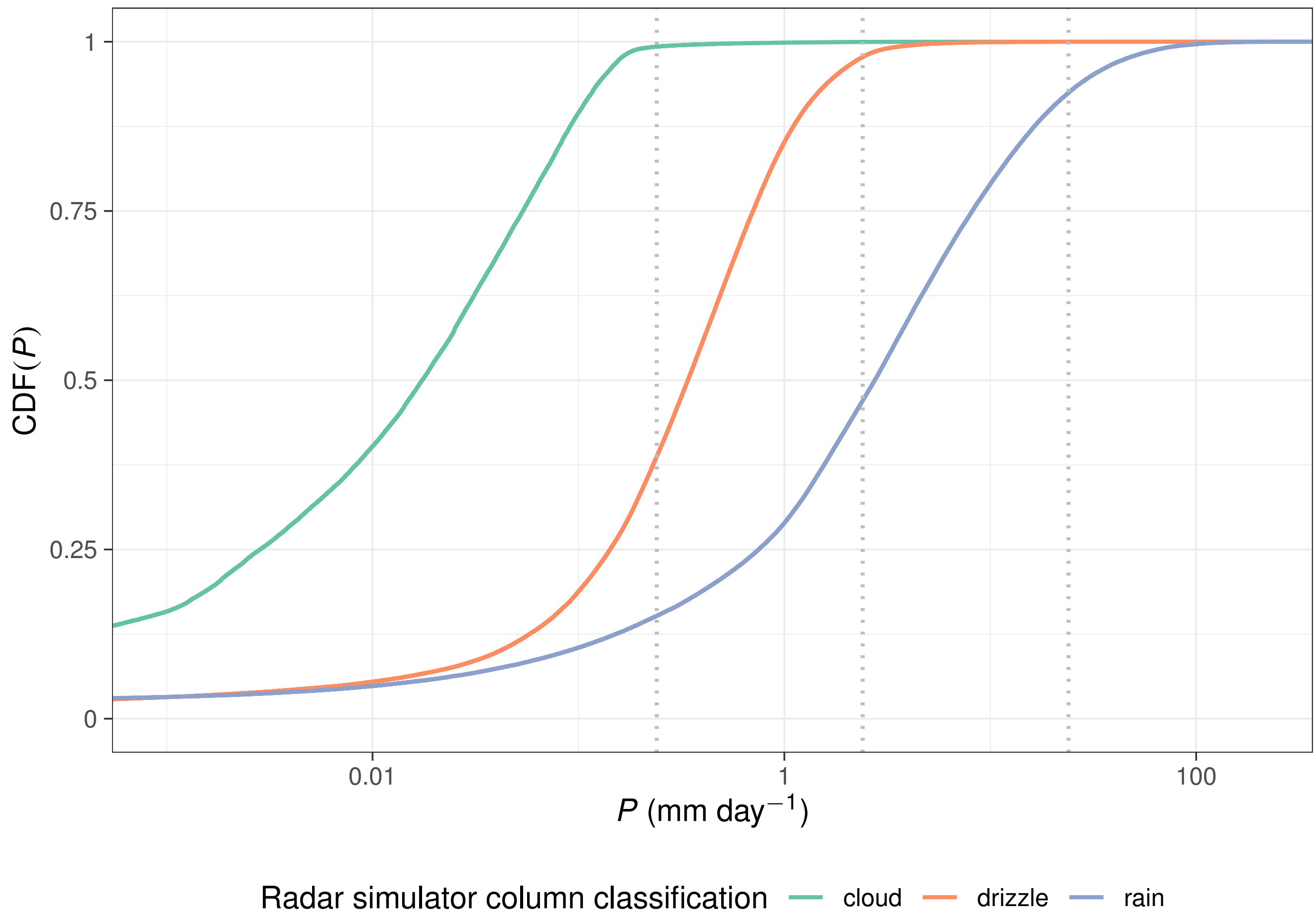

Figure S9. Correspondence between simulated radar reflectivity and surface precipitation rate.
Cumulative distribution functions (CDFs) of surface precipitation rate P by radar-simulator reflectivity-based classification of the column as cloudy, drizzling, or rainy show that reflectivity-based intensity classifications correspond closely with surface precipitation rate. The gray dashed lines correspond to 0.01, 0.1, and 1 mm h^{-1}.

Table S1. Rapid adjustments and cloud state (global mean) across experiments.
Compared to the reference model, the reduced scaling factor configurations estimate a weaker normalized adjustment $F_{\mathcal{L}}/F_{N_d}$, while the increased threshold r_e configurations estimate a stronger normalized adjustment. The large TOA radiative imbalance R_{TOA} in the reference run is a result of nudging; the non-nudged version of the reference run for the same time period has a more plausible $R_{\mathrm{TOA}} = 0.34\ \mathrm{W\,m^{-2}}$. Despite large changes in warm cloud properties, the ice water path $\mathcal{I}$ changes are within approximately 1%.

	ERF contributions (W m^{-2})			State variables			
Case	F_{N_d}	$F_{\mathcal{L}}$	$F_{\mathcal{L}}/F_{N_d}$	R_{TOA} (W m^{-2})	$\mathcal{S}_c$ (W m^{-2})	$\mathcal{I}$ (g m^{-2})	$\mathcal{L}$ (g m^{-2})
$Q_{\mathrm{aut}} \times 0.04$	−0.66	−0.57	0.87	−9.98	−58.97	10.56	214
$Q_{\mathrm{aut}} \times 0.1$	−0.65	−0.59	0.91	−8.23	−57.10	10.55	184
$Q_{\mathrm{aut}} \times 0.4$	−0.62	−0.64	1.02	−4.76	−53.33	10.53	139
$Q_{\mathrm{aut}} \times 1$	−0.59	−0.64	1.07	−1.93	−50.24	10.50	110
Reference	−0.52	−0.57	1.08	2.89	−44.95	10.45	73
$r_e > 10$ µm	−0.51	−0.59	1.15	2.82	−45.04	10.45	73
$r_e > 12$ µm	−0.52	−0.61	1.17	2.41	−45.46	10.46	76
$r_e > 15$ µm	−0.59	−0.73	1.24	0.26	−47.84	10.50	92
$r_e > 17$ µm	−0.65	−0.81	1.25	−2.31	−50.60	10.52	114

Table S2. Rapid adjustments and cloud state (global mean) across experiments scanning α.
This table reprises Table S1 but varies α.

	ERF contributions (W m^{-2})			State variables		
Case	F_{N_d}	$F_{\mathcal{L}}$	$F_{\mathcal{L}}/F_{N_d}$	R_{TOA} (W m^{-2})	$\mathcal{S}_c$ (W m^{-2})	$\mathcal{L}$ (g m^{-2})
$\alpha = 1.75$	−0.09	−0.30	3.30	25.80	−17.75	2
$\alpha = 2$	−0.24	−0.42	1.77	18.39	−27.80	13
$\alpha = 2.25$	−0.38	−0.50	1.32	9.71	−37.50	38
$\alpha = 2.47$ (reference)	−0.52	−0.57	1.08	2.89	−44.95	73
$\alpha = 2.8$	−0.62	−0.60	0.96	−4.84	−53.43	139
$\alpha = 3.2$	−0.65	−0.52	0.79	−10.01	−59.01	215
$\alpha = 3.6$	−0.65	−0.46	0.70	−12.35	−61.49	270
$\alpha = 4$	−0.65	−0.45	0.69	−13.67	−62.98	308
$\alpha = 4.5$	−0.64	−0.40	0.62	−14.71	−64.16	340
$\alpha = 5$	−0.64	−0.37	0.58	−15.36	−64.91	361

Table S3. Rapid adjustments and cloud state (global mean) across experiments scanning β.
This table reprises Table S1 but varies β.

	ERF contributions (W m^{-2})			State variables		
Case	F_{N_d}	$F_{\mathcal{L}}$	$F_{\mathcal{L}}/F_{N_d}$	R_{TOA} (W m^{-2})	$\mathcal{S}_c$ (W m^{-2})	$\mathcal{L}$ (g m^{-2})
$\beta = 1$	−0.23	−0.24	1.06	14.59	−32.23	21
$\beta = 1.2$	−0.29	−0.31	1.07	11.79	−35.28	30
$\beta = 1.4$	−0.36	−0.38	1.08	8.80	−38.51	41
$\beta = 1.6$	−0.42	−0.46	1.09	5.82	−41.78	56
$\beta = 1.79$ (reference)	−0.52	−0.57	1.08	2.89	−44.95	73
$\beta = 2$	−0.58	−0.67	1.17	−0.23	−48.35	95
$\beta = 2.4$	−0.65	−0.75	1.15	−5.50	−54.07	147
$\beta = 2.8$	−0.68	−0.75	1.10	−9.31	−58.20	202
$\beta = 3.2$	−0.67	−0.68	1.01	−11.72	−60.85	252
$\beta = 3.6$	−0.64	−0.47	0.75	−13.11	−62.36	291

REFERENCES

1. O. Boucher, D. Randall, P. Artaxo, C. Bretherton, G. Feingold, P. Forster, V.-M. Kerminen, Y. Kondo, H. Liao, U. Lohmann, P. Rasch, S. Satheesh, S. Sherwood, B. Stevens, X. Zhang, *Clouds and Aerosols* (Cambridge Univ. Press, Cambridge, United Kingdom and New York, NY, USA, 2014), book section Chap. 7, pp. 571–658.
2. S. Twomey, Influence of pollution on shortwave albedo of clouds. *J. Atmos. Sci.* **34**, 1149–1152 (1977).
3. J. Quaas, O. Boucher, N. Bellouin, S. Kinne, Satellite-based estimate of the direct and indirect aerosol climate forcing. *J. Geophys. Res.* **113**, 05204 (2008).
4. N. Bellouin, J. Quaas, E. Gryspeerdt, S. Kinne, P. Stier, D. Watson-Parris, O. Boucher, K. Carslaw, M. Christensen, A.-L. Daniau, J.-L. Dufresne, G. Feingold, S. Fiedler, P. Forster, A. Gettelman, J. M. Haywood, F. Malavelle, U. Lohmann, T. Mauritsen, D. McCoy, G. Myhre, J. Mülmenstädt, D. Neubauer, A. Possner, M. Rugenstein, Y. Sato, M. Schulz, S. E. Schwartz, O. Sourdeval, T. Storelvmo, V. Toll, D. Winker, B. Stevens, Bounding global aerosol radiative forcing of climate change. *Rev. Geophys.* **58**, e2019RG000660 (2020).
5. E. Gryspeerdt, J. Quaas, S. Ferrachat, A. Gettelman, S. Ghan, U. Lohmann, H. Morrison, D. Neubauer, D. G. Partridge, P. Stier, T. Takemura, H. Wang, M. Wang, K. Zhang, Constraining the instantaneous aerosol influence on cloud albedo. *Proc. Natl. Acad. Sci. U.S.A.* **114**, 4899–4904 (2017).
6. B. A. Albrecht, Aerosols, cloud microphysics, and fractional cloudiness. *Science* **245**, 1227–1230 (1989).
7. R. Pincus, M. B. Baker, Effect of precipitation on the albedo susceptibility of clouds in the marine boundary-layer. *Nature* **372**, 250–252 (1994).
8. A. S. Ackerman, M. P. Kirkpatrick, D. Stevens, O. Toon, The impact of humidity above stratiform clouds on indirect aerosol climate forcing. *Nature* **432**, 1014–1017 (2004).
9. C. S. Bretherton, P. N. Blossey, J. Uchida, Cloud droplet sedimentation, entrainment efficiency, and subtropical stratocumulus albedo. *Geophys. Res. Lett.* **34**, L03813 (2007).
10. J. D. Small, P. Y. Chuang, G. Feingold, H. Jiang, Can aerosol decrease cloud lifetime? *Geophys. Res. Lett.* **36**, L16806 (2009).
11. A. Seifert, T. Heus, R. Pincus, B. Stevens, Large-eddy simulation of the transient and near-equilibrium behavior of precipitating shallow convection. *J. Adv. Model. Earth Syst.* **7**, 1918–1937 (2015).

12. V. Toll, M. Christensen, J. Quaas, N. Bellouin, Weak average liquid-cloud-water response to anthropogenic aerosols. *Nature* **572**, 51−55 (2019).
13. E. Gryspeerdt, T. Goren, O. Sourdeval, J. Quaas, J. Muelmenstaedt, S. Dipu, C. Unglaub, A. Gettelman, M. Christensen, Constraining the aerosol influence on cloud liquid water path. *Atmos. Chem. Phys.* **19**, 5331–5347 (2019).
14. A. Gettelman, Putting the clouds back in aerosol-cloud interactions. *Atmos. Chem. Phys.* **15**, 12397–12411 (2015).
15. H. Takahashi, M. Lebsock, K. Suzuki, G. Stephens, M. Wang, An investigation of microphysics and subgrid-scale variability in warm-rain clouds using the a-train observations and a multiscale modeling framework. *J. Geophys. Res.* **122**, 7493–7504 (2017).
16. K. Suzuki, G. Stephens, A. Bodas-Salcedo, M. Wang, J.-C. Golaz, T. Yokohata, T. Koshiro, Evaluation of the warm rain formation process in global models with satellite observations. *J. Atmos. Sci.* **72**, 3996–4014 (2015).
17. G. J. Kooperman, M. S. Pritchard, T. A. O'Brien, B. W. Timmermans, Rainfall from resolved rather than parameterized processes better represents the present-day and climate change response of moderate rates in the community atmosphere model. *J. Adv. Model. Earth Syst.* **10**, 971–988 (2018).
18. U. Lohmann, S. Ferrachat, Impact of parametric uncertainties on the present-day climate and on the anthropogenic aerosol effect. *Atmos. Chem. Phys.* **10**, 11373–11383 (2010).
19. J.-C. Golaz, M. Salzmann, L. J. Donner, L. W. Horowitz, Y. Ming, M. Zhao, Sensitivity of the aerosol indirect effect to subgrid variability in the cloud parameterization of the gfdl atmosphere general circulation model am3. *J. Clim.* **24**, 3145–3160 (2011).
20. T. Mauritsen, B. Stevens, E. Roeckner, T. Crueger, M. Esch, M. Giorgetta, H. Haak, J. Jungclaus, D. Klocke, D. Matei, U. Mikolajewicz, D. Notz, R. Pincus, H. Schmidt, L. Tomassini, Tuning the climate of a global model. *J. Adv. Model. Earth Syst.* **4**, M00A01 (2012).
21. G. L. Stephens, T. L'Ecuyer, R. Forbes, A. Gettleman, J.-C. Golaz, A. Bodas-Salcedo, K. Suzuki, P. Gabriel, J. Haynes, Dreary state of precipitation in global models. *J. Geophys. Res.* **115**, D24211 (2010).
22. U. Lohmann, J. Quaas, S. Kinne, J. Feichter, Different approaches for constraining global climate models of the anthropogenic indirect aerosol effect. *Bull. Am. Meteorol. Soc.* **88**, 243−250 (2007).
23. L. von Bertalanffy, The theory of open systems in physics and biology. *Science* **111**, 23–29 (1950).
24. L. A. Lee, C. L. Reddington, K. S. Carslaw, On the relationship between aerosol model uncertainty and radiative forcing uncertainty. *Proc. Natl. Acad. Sci. U.S.A.* **113**, 5820–5827 (2016).

25. L. A. Regayre, J. S. Johnson, M. Yoshioka, K. J. Pringle, D. M. H. Sexton, B. B. B. Booth, L. A. Lee, N. Bellouin, K. S. Carslaw, Aerosol and physical atmosphere model parameters are both important sources of uncertainty in aerosol erf. *Atmos. Chem. Phys.* **18**, 9975–10006 (2018).
26. J. Quaas, Y. Ming, S. Menon, T. Takemura, M. Wang, J. E. Penner, A. Gettelman, U. Lohmann, N. Bellouin, O. Boucher, A. M. Sayer, G. E. Thomas, A. McComiskey, G. Feingold, C. Hoose, J. E. Kristjansson, X. Liu, Y. Balkanski, L. J. Donner, P. A. Ginoux, P. Stier, B. Grandey, J. Feichter, I. Sednev, S. E. Bauer, D. Koch, R. G. Grainger, A. Kirkevag, T. Iversen, O. Seland, R. Easter, S. J. Ghan, P. J. Rasch, H. Morrison, J. F. Lamarque, M. J. Iacono, S. Kinne, M. Schulz, Aerosol indirect effects - general circulation model intercomparison and evaluation with satellite data. *Atmos. Chem. Phys.* **9**, 8697–8717 (2009).
27. M. Wang, S. Ghan, X. Liu, T. S. L'Ecuyer, K. Zhang, H. Morrison, M. Ovchinnikov, R. Easter, R. Marchand, D. Chand, Y. Qian, J. E. Penner, Constraining cloud lifetime effects of aerosols using a-train satellite observations. *Geophys. Res. Lett.* **39**, L15709 (2012).
28. Z. J. Lebo, G. Feingold, On the relationship between responses in cloud water and precipitation to changes in aerosol. *Atmos. Chem. Phys.* **14**, 11817–11831 (2014).
29. P.-L. Ma, P. J. Rasch, H. Chepfer, D. M. Winker, S. J. Ghan, Observational constraint on cloud susceptibility weakened by aerosol retrieval limitations. *Nat. Commun.* **9**, 2640 (2018).
30. J. Mülmenstädt, O. Sourdeval, J. Delanoë, J. Quaas, Frequency of occurrence of rain from liquid-, mixed-, and ice-phase clouds derived from a-train satellite retrievals. *Geophys. Res. Lett.* **42**, 6502–6509 (2015).
31. P. R. Field, A. J. Heymsfield, Importance of snow to global precipitation. *Geophys. Res. Lett.* **42**, 9512–9520 (2015).
32. E. Kessler, *On the Distribution and Continuity of Water Substance in Atmospheric Circulations* (American Meteorological Society, Boston, MA, 1969), pp. 1–84.
33. F. F. Malavelle, J. M. Haywood, A. Jones, A. Gettelman, L. C. Larisse, S. Bauduin, R. P. Allan, I. H. H. Karset, J. E. Kristjansson, L. Oreopoulos, N. C. Ho, D. Lee, N. Bellouin, O. Boucher, D. P. Grosvenor, K. S. Carslaw, S. Dhomse, G. W. Mann, A. Schmidt, H. Coe, M. E. Hartley, M. Dalvi, A. A. Hill, B. T. Johnson, C. E. Johnson, J. R. Knight, F. M. O'Connor, D. G. Partridge, P. Stier, G. Myhre, S. Platnick, G. L. Stephens, H. Takahashi, T. Thordarson, Strong constraints on aerosol-cloud interactions from volcanic eruptions. *Nature* **546**, 485–491 (2017).
34. D. T. McCoy, D. L. Hartmann, M. D. Zelinka, P. Ceppi, D. P. Grosvenor, Mixed-phase cloud physics and southern ocean cloud feedback in climate models. *J. Geophys. Res.* **120**, 9539–9554 (2015).

35. I. Tan, T. Storelvmo, M. D. Zelinka, Observational constraints on mixed-phase clouds imply higher climate sensitivity. *Science* **352**, 224–227 (2016).
36. J. E. Kay, L. Bourdages, N. B. Miller, A. Morrison, V. Yettella, H. Chepfer, B. Eaton, Evaluating and improving cloud phase in the community atmosphere model version 5 using spaceborne lidar observations. *J. Geophys. Res.* **121**, 4162–4176 (2016).
37. A. Bodas-Salcedo, T. Andrews, A. V. Karmalkar, M. A. Ringer, Cloud liquid water path and radiative feedbacks over the southern ocean. *Geophys. Res. Lett.* **43**, 10938–10946 (2016).
38. W. R. Frey, J. E. Kay, The influence of extratropical cloud phase and amount feedbacks on climate sensitivity. *Clim. Dyn.* **50**, 3097–3116 (2018).
39. L. D. Rotstayn, Y. Liu, A smaller global estimate of the second indirect aerosol effect. *Geophys. Res. Lett.* **32**, L05708 (2005).
40. M. D. Zelinka, T. Andrews, P. M. Forster, K. E. Taylor, Quantifying components of aerosol-cloud-radiation interactions in climate models. *J. Geophys. Res.* **119**, 7599–7615 (2014).
41. J. Mülmenstädt, E. Gryspeerdt, M. Salzmann, P.-L. Ma, S. Dipu, J. Quaas, Separating radiative forcing by aerosol-cloud interactions and fast cloud adjustments in the echam-hammoz aerosol-climate model using the method of partial radiative perturbations. *Atmos. Chem. Phys.* **19**, 15415–15429 (2019).
42. E. Gryspeerdt, J. Muelmenstadt, A. Gettelman, F. F. Malavelle, H. Morrison, D. Neubauer, D. G. Partridge, P. Stier, T. Takemura, H. Wang, M. Wang, K. Zhang, Surprising similarities in model and observational aerosol radiative forcing estimates. *Atmos. Chem. Phys.* **20**, 613–623 (2020).
43. H. Song, Z. Zhang, P.-L. Ma, S. Ghan, M. Wang, The importance of considering sub-grid cloud variability when using satellite observations to evaluate the cloud and precipitation simulations in climate models. *Geosci. Model Dev.* **11**, 3147–3158 (2018).
44. J. E. Kay, T. L'Ecuyer, A. Pendergrass, H. Chepfer, R. Guzman, V. Yettella, Scale-aware and definition-aware evaluation of modeled near-surface precipitation frequency using cloudsat observations. *J. Geophys. Res.* **123**, 4294–4309 (2018).
45. G. Stephens, D. Winker, J. Pelon, C. Trepte, D. Vane, C. Yuhas, T. L'Ecuyer, M. Lebsock, Cloudsat and calipso within the a-train: Ten years of actively observing the earth system. *Bull. Am. Meteorol. Soc.* **99**, 569–581 (2018).
46. A. J. Illingworth, H. W. Barker, A. Beljaars, M. Ceccaldi, H. Chepfer, N. Clerbaux, J. Cole, J. Delanoe, C. Domenech, D. P. Donovan, S. Fukuda, M. Hirakata, R. J. Hogan, A. Huenerbein, P. Kollias, T. Kubota, T. Nakajima, T. Y. Nakajima, T. Nishizawa, Y. Ohno, H. Okamoto, R. Oki, K. Sato, M. Satoh, M. W. Shephard, A. Velazquez-Blazquez, U. Wandinger, T. Wehr, G.-J. van

Zadelhoff, The earthcare satellite the next step forward in global measurements of clouds, aerosols, precipitation, and radiation. *Bull. Am. Meteorol. Soc.* **96**, 1311–1332 (2015).

47. National Academies of Sciences, Engineering, and Medicine, *Thriving on Our Changing Planet: A Decadal Strategy for Earth Observation from Space* (The National Academies Press, Washington, DC, 2018).
48. D. Neubauer, U. Lohmann, C. Hoose, M. G. Frontoso, Impact of the representation of marine stratocumulus clouds on the anthropogenic aerosol effect. *Atmos. Chem. Phys.* **14**, 11997–12022 (2014).
49. B. Stevens, M. Giorgetta, M. Esch, T. Mauritsen, T. Crueger, S. Rast, M. Salzmann, H. Schmidt, J. Bader, K. Block, R. Brokopf, I. Fast, S. Kinne, L. Kornblueh, U. Lohmann, R. Pincus, T. Reichler, E. Roeckner, Atmospheric component of the mpi-m earth system model: Echam6. *J. Adv. Model. Earth Syst.* **5**, 146–172 (2013).
50. P. Stier, J. Feichter, S. Kinne, S. Kloster, E. Vignati, J.Wilson, L. Ganzeveld, I. Tegen, M.Werner, Y. Balkanski, M. Schulz, O. Boucher, A. Minikin, A. Petzold, The aerosol-climate model echam5-ham. *Atmos. Chem. Phys.* **5**, 1125–1156 (2005).
51. K. Zhang, D. O'Donnell, J. Kazil, P. Stier, S. Kinne, U. Lohmann, S. Ferrachat, B. Croft, J. Quaas, H. Wan, S. Rast, J. Feichter, The global aerosol-climate model echam-ham, version 2: Sensitivity to improvements in process representations. *Atmos. Chem. Phys.* **12**, 8911–8949 (2012).
52. D. E. Kinnison, G. P. Brasseur, S. Walters, R. R. Garcia, D. R. Marsh, F. Sassi, V. L. Harvey, C. E. Randall, L. Emmons, J. F. Lamarque, P. Hess, J. J. Orlando, X. X. Tie, W. Randel, L. L. Pan, A. Gettelman, C. Granier, T. Diehl, U. Niemeier, A. J. Simmons, Sensitivity of chemical tracers to meteorological parameters in the mozart-3 chemical transport model. *J. Geophys. Res.* **112**, D20302 (2007).
53. U. Lohmann, E. Roeckner, Design and performance of a new cloud microphysics scheme developed for the echam general circulation model. *Clim. Dyn.* **12**, 557–572 (1996).
54. U. Lohmann, P. Stier, C. Hoose, S. Ferrachat, S. Kloster, E. Roeckner, J. Zhang, Cloud microphysics and aerosol indirect effects in the global climate model echam5-ham. *Atmos. Chem. Phys.* **7**, 3425–3446 (2007).
55. U. Lohmann, C. Hoose, Sensitivity studies of different aerosol indirect effects in mixed-phase clouds. *Atmos. Chem. Phys.* **9**, 8917–8934 (2009).
56. M. Tiedtke, A comprehensive mass flux scheme for cumulus parameterization in large-scale models. *Mon. Weather Rev.* **117**, 1779–1800 (1989).

57. M. Khairoutdinov, Y. Kogan, A new cloud physics parameterization in a large-eddy simulation model of marine stratocumulus. *Mon. Weather Rev.* **128**, 229–243 (2000).
58. L. D. Rotstayn, On the "tuning" of autoconversion parameterizations in climate models. *J. Geophys. Res.* **105**, 15495–15507 (2000).
59. T. Weber, J. Quaas, Incorporating the subgrid-scale variability of clouds in the autoconversion parameterization using a pdf-scheme. *J. Adv. Model. Earth Syst.* **4**, M11003 (2012).
60. M. Lebsock, H. Morrison, A. Gettelman, Microphysical implications of cloud-precipitation covariance derived from satellite remote sensing. *J. Geophys. Res.* **118**, 6521–6533 (2013).
61. Z. Zhang, H. Song, P.-L. Ma, V. E. Larson, M. Wang, X. Dong, J. Wang, Subgrid variations of the cloud water and droplet number concentration over the tropical ocean: satellite observations and implications for warm rain simulations in climate models. *Atmos. Chem. Phys.* **19**, 1077–1096 (2019).
62. H. Sundqvist, E. Berge, J. Kristjánsson, Condensation and cloud parameterization studies with a mesoscale numerical weather prediction model. *Mon. Weather Rev.* **117**, 1641–1657 (1989).
63. J. M. Haynes, T. S. L'Ecuyer, G. L. Stephens, S. D. Miller, C. Mitrescu, N. B. Wood, S. Tanelli, Rainfall retrieval over the ocean with spaceborne W-band radar. *J. Geophys. Res.* **114**, D00A22 (2009).
64. M. Smalley, T. L'Ecuyer, M. Lebsock, J. Haynes, A comparison of precipitation occurrence from the ncep stage iv qpe product and the cloudsat cloud profiling radar. *J. Hydrometeorol.* **15**, 444–458 (2014).
65. C. Schumacher, R. A. Houze Jr., Comparison of radar data from the trmm satellite and kwajalein oceanic validation site. *J. Appl. Meteorol.* **39**, 2151–2164 (2000).
66. A. Bodas-Salcedo, M. J. Webb, S. Bony, H. Chepfer, J.-L. Dufresne, S. A. Klein, Y. Zhang, R. Marchand, J. M. Haynes, R. Pincus, V. O. John, Cosp satellite simulation software for model assessment. *Bull. Am. Meteorol. Soc.* **92**, 1023–1043 (2011).
67. C. C. W. Nam, J. Quaas, Evaluation of clouds and precipitation in the echam5 general circulation model using calipso and cloudsat satellite data. *J. Clim.* **25**, 4975–4992 (2012).
68. J. M. Haynes, R. T. Marchand, Z. Luo, A. Bodas-Salcedo, G. L. Stephens, A multipurpose radar simulation package: Quickbeam. *Bull. Am. Meteorol. Soc.* **88**, 1723−1728 (2007).
69. K. Thayer-Calder, A. Gettelman, C. Craig, S. Goldhaber, P. A. Bogenschutz, C.-C. Chen, H. Morrison, J. Hoeft, E. Raut, B. M. Griffin, J. K. Weber, V. E. Larson, M. C. Wyant, M. Wang, Z. Guo, S. J. Ghan, A unified parameterization of clouds and turbulence using clubb and subcolumns in the community atmosphere model. *Geosci. Model Dev.* **8**, 3801–3821 (2015).

70. G. J. Tripoli, W. R. Cotton, A numerical investigation of several factors contributing to the observed variable intensity of deep convection over south florida. *J. Appl. Meteorol.* **19**, 1037–1063 (1980).
71. Y. Liu, P. H. Daum, Parameterization of the autoconversion process. part i: Analytical formulation of the kessler-type parameterizations. *J. Atmos. Sci.* **61**, 1539–1548 (2004).
72. D. P. Dee, S. M. Uppala, A. J. Simmons, P. Berrisford, P. Poli, S. Kobayashi, U. Andrae, M. A. Balmaseda, G. Balsamo, P. Bauer, P. Bechtold, A. C. M. Beljaars, L. van de Berg, J. Bidlot, N. Bormann, C. Delsol, R. Dragani, M. Fuentes, A. J. Geer, L. Haimberger, S. B. Healy, H. Hersbach, E. V. Holm, L. Isaksen, P. Kallberg, M. Koehler, M. Matricardi, A. P. McNally, B. M. Monge-Sanz, J.-J. Morcrette, B.-K. Park, C. Peubey, P. de Rosnay, C. Tavolato, J.-N. Thepaut, F. Vitart, The era-interim reanalysis: configuration and performance of the data assimilation system. *Q. J. R. Meteorol. Soc.* **137**, 553–597 (2011).
73. G. J. Kooperman, M. S. Pritchard, S. J. Ghan, M. Wang, R. C. J. Somerville, L. M. Russell, Constraining the influence of natural variability to improve estimates of global aerosol indirect effects in a nudged version of the community atmosphere model 5. *J. Geophys. Res.* **117**, D23204 (2012).
74. K. Zhang, H. Wan, X. Liu, S. J. Ghan, G. J. Kooperman, P.-L. Ma, P. J. Rasch, D. Neubauer, U. Lohmann, Technical note: On the use of nudging for aerosol-climate model intercomparison studies. *Atmos. Chem. Phys.* **14**, 8631–8645 (2014).
75. S. Wang, Q. Wang, G. Feingold, Turbulence, condensation, and liquid water transport in numerically simulated nonprecipitating stratocumulus clouds. *J. Atmos. Sci.* **60**, 262–278 (2003).
76. A. A. Hill, G. Feingold, H. Jiang, The influence of entrainment and mixing assumption on aerosol-cloud interactions in marine stratocumulus. *J. Atmos. Sci.* **66**, 1450–1464 (2009).
77. H. Xue, G. Feingold, Large-eddy simulations of trade wind cumuli: Investigation of aerosol indirect effects. *J. Atmos. Sci.* **63**, 1605–1622 (2006).
78. H. Xue, G. Feingold, B. Stevens, Aerosol effects on clouds, precipitation, and the organization of shallow cumulus convection. *J. Atmos. Sci.* **65**, 392–406 (2008).
79. B. Stevens, G. Feingold, Untangling aerosol effects on clouds and precipitation in a buffered system. *Nature* **461**, 607–613 (2009).
80. M. Salzmann, Y. Ming, J.-C. Golaz, P. A. Ginoux, H. Morrison, A. Gettelman, M. Kraemer, L. J. Donner, Two-moment bulk stratiform cloud microphysics in the gfdl am3 gcm: description, evaluation, and sensitivity tests. *Atmos. Chem. Phys.* **10**, 8037–8064 (2010).
81. H. Guo, J.-C. Golaz, L. J. Donner, Aerosol effects on stratocumulus water paths in a pdf-based parameterization. *Geophys. Res. Lett.* **38**, L17808 (2011).

82. C. Zhou, J. E. Penner, Why do general circulation models overestimate the aerosol cloud lifetime effect?: A case study comparing cam5 and a crm. *Atmos. Chem. Phys.* **17**, 21–29 (2017).
83. J.Mülmenstädt, G. Feingold, The radiative forcing of aerosol–cloud interactions in liquid clouds:Wrestling and embracing uncertainty. *Curr. Clim. Change Rep.* **4**, 23–40 (2018).
84. I. A. Boutle, S. J. Abel, P. G. Hill, C. J. Morcrette, Spatial variability of liquid cloud and rain: observations and microphysical effects. *Q. J. R. Meteorol. Soc.* **140**, 583–594 (2014).
85. R.Wood, Drizzle in stratiform boundary layer clouds. part ii: Microphysical aspects. *J. Atmos. Sci.* **62**, 3034–3050 (2005).
86. T. Michibata, T. Takemura, Evaluation of autoconversion schemes in a single model framework with satellite observations. *J. Geophys. Res.* **120**, 9570–9590 (2015).
87. A. Sorooshian, G. Feingold, M. D. Lebsock, H. Jiang, G. L. Stephens, On the precipitation susceptibility of clouds to aerosol perturbations. *Geophys. Res. Lett.* **36**, L13803 (2009).
88. U. Lohmann, J. Feichter, Impact of sulfate aerosols on albedo and lifetime of clouds: A sensitivity study with the echam4 gcm. *J. Geophys. Res.* **102**, 13685–13700 (1997).
89. X. Jing, K. Suzuki, T. Michibata, The key role of warm rain parameterization in determining the aerosol indirect effect in a global climate model. *J. Clim.* **32**, 4409–4430 (2019).
90. J. E. Penner, J. Quaas, T. Storelvmo, T. Takemura, O. Boucher, H. Guo, A. Kirkevag, J. E. Kristjansson, Ø. Seland, Model intercomparison of indirect aerosol effects. *Atmos. Chem. Phys.* **6**, 3391–3405 (2006).
91. H. Jiang, G. Feingold, A. Sorooshian, Effect of aerosol on the susceptibility and efficiency of precipitation in warm trade cumulus clouds. *J. Atmos. Sci.* **67**, 3525–3540 (2010).
92. F. Glassmeier, U. Lohmann, Constraining precipitation susceptibility of warm-, ice-, and mixed-phase clouds with microphysical equations. *J. Atmos. Sci.* **73**, 5003–5023 (2016).
93. A. Gettelman, H. Morrison, C. R. Terai, R. Wood, Microphysical process rates and global aerosol-cloud interactions. *Atmos. Chem. Phys.* **13**, 9855–9867 (2013).